Separation and Purification Technology 209 (2019) 229–237

Contents lists available at ScienceDirect

Separation and Purification Technology

journal homepage: www.elsevier.com/locate/seppur

Mass transfer studies on the dehydration of supercritical carbon dioxide using dense polymeric membranes

Andrew Shamu[a,b], Henk Miedema[a], Sybrand J. Metz[a], Zandrie Borneman[b,c], Kitty Nijmeijer[b,c,*]

[a] Wetsus, Centre of Excellence for Sustainable Water Technology, Oostergoweg 9, 8911 MA Leeuwarden, The Netherlands
[b] Membrane Materials and Processes, Eindhoven University of Technology, P.O. Box 513, 5600 MB Eindhoven, The Netherlands
[c] Dutch Institute for Fundamental Energy Research (DIFFER), De Zaale 20, 5612 AJ Eindhoven, The Netherlands

ARTICLE INFO

Keywords:
Supercritical fluids
Carbon dioxide
Gas separation
Membranes
Concentration polarization

ABSTRACT

Continuous drying processes using supercritical CO_2 ($scCO_2$) as a water extraction agent require 24/7 operational dehydration units for $scCO_2$ regeneration. Dehydration units using dense polymeric membranes are considered a cost effective, sustainable alternative to the current zeolite-based units. The focus of previous studies on the membrane-based dehydration of $scCO_2$ was always on the membrane itself whereas boundary layer effects, e.g., concentration polarization, were not taken into account. To quantify the boundary layer effects, simulations were performed using three different membrane materials: SPEEK, Nafion® 117, and PEBAX® 1074. Process conditions during the simulations ranged from 8.0 to 18.0 MPa and 40 to 100 °C. Even though the three types of membranes examined differ in their H_2O permeability and H_2O over CO_2 selectivity, in all cases 80% of the total mass-transfer resistance can be assigned to concentration polarization effects, making it the dominant parameter for water transport. Despite high but differing intrinsic water permeabilities of all three membranes materials, the H_2O transport, thus H_2O flux through the membrane is significantly reduced by concentration polarization down to similar levels. This makes it necessary to use larger membrane areas, that result in higher CO_2 fluxes. As a consequence, material selection is predominantly based on the ability to reject CO_2. Optimization of process conditions other than membrane material is briefly discussed.

1. Introduction

Supercritical CO_2 ($scCO_2$) is frequently used in industrial processes for e.g. the drying of fruits and vegetables to extent shelf life [1]. Due to its supercritical state, it has high densities values typical for liquids and simultaneously low viscosities characteristic for gases [2]. Moreover as drying is performed at relatively low temperatures and under oxygen free conditions, vitamins, pigments and proteins are preserved ensuring the nutritional value and the dried products keep their color, shape, structure and texture [3]. Although performed under pressure, $scCO_2$ drying is a very mild process.

Fig. 1 displays the typical outline of such an industrial drying process using $scCO_2$. Dry $scCO_2$ enters the extraction unit, extracts the water from the product and leaves the unit as a humidified stream. This stream is then regenerated in a dehydration unit before it is re-injected into the extraction unit for the next water extraction cycle. Typical fluid temperatures and pressures are in the range of 45 °C and 13.0 MPa [3], which is beyond carbon dioxides critical values of T = 31.04 °C and p = 7.38 MPa [2].

Currently, columns packed with adsorbents such as zeolites are applied to dehydrate the $scCO_2$. The enclosed adsorbents extract water from the $scCO_2$ until they are fully saturated. Temperatures up to 260 °C are needed to reactivate the zeolite by water desorption [4]. While this energy demanding reactivation step is carried out, a second zeolite packed column is switched in to continue the $scCO_2$ dehydration. The required reactivation energy and the additional zeolite column make the $scCO_2$ drying process economically less attractive. Lohaus et al. [4] showed with their model, based on Scholz et al. [5], that a shift towards a membrane-based dehydration process, where a second dehydration unit and reactivation steps are obsolete, could reduce the dehydration costs up to 20%. Even though Lohaus et al. simulated and discussed water vapor concentration profiles and the driving force profiles along the membrane unit, the combined mass transfer of the skin layer material, its porous support and the feed- and permeate boundary layers were not taken into account in their analysis. Each of these stacked layers is very different constituted, especially under highly pressurized $scCO_2$ conditions, where the fluids density and viscosity are very different to those in conventional gas separation applications. It stands to

* Corresponding author at: Membrane Materials and Processes, Eindhoven University of Technology, P.O. Box 513, 5600 MB Eindhoven, The Netherlands.
E-mail address: d.c.nijmeijer@tue.nl (K. Nijmeijer).

https://doi.org/10.1016/j.seppur.2018.07.042
Received 13 November 2017; Received in revised form 16 July 2018; Accepted 16 July 2018
Available online 17 July 2018

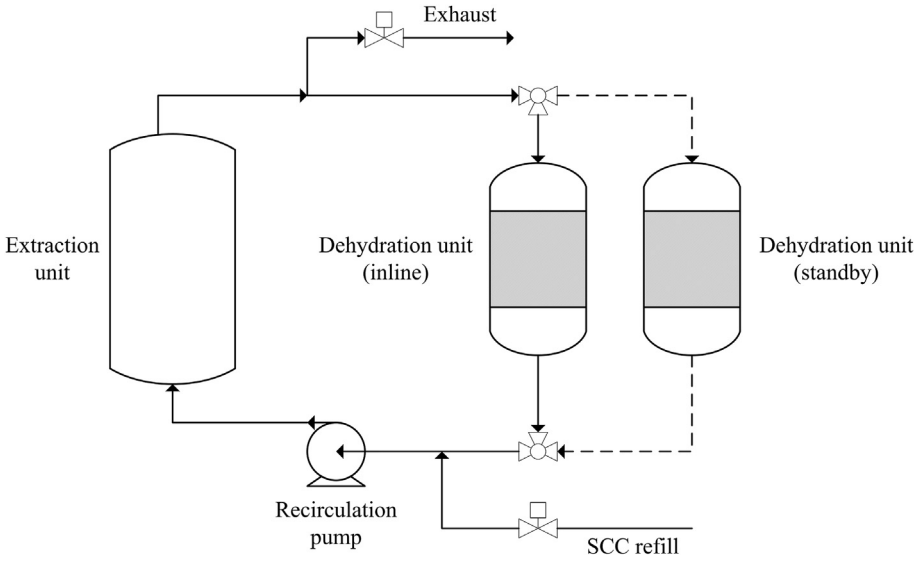

Fig. 1. Schematic view of a typical currently existing dehydration process using $scCO_2$ as the water-extraction agent (left unit) and zeolite to dehydrate (regenerate) $scCO_2$ (right units). To enable continuous regeneration a second dehydration unit is in standby mode.

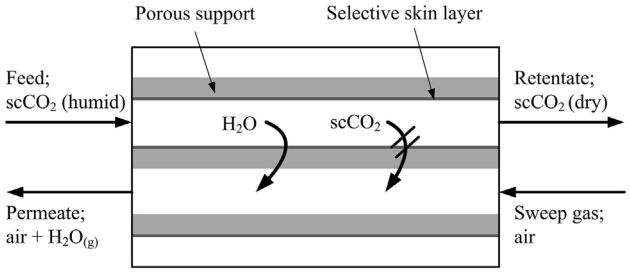

Fig. 2. Scheme of the flat sheet membrane stack considered for the mass transfer examination. Water, enters the unit via the humid feed stream and permeates through the skin layer while $scCO_2$ is rejected. This leads to a gradual decay of the water content within the feed stream. The permeated water is entrained by the dry air entering the unit as a sweep gas. The dried $scCO_2$ is ready for its reuse as an extraction agent whereas the humidified air is emitted into the environment.

reason that in the special case of exposure to $scCO_2$ the contribution of each single layer contributes differently to the total water transport resistance and thus to the water permeance.

Composite membranes, consisting of a thick porous support and a thin selective, water permeable, skin layer, can withstand transmembrane pressures of more than 10.0 MPa. Due to polarization effects in the boundary layers, evoked by severe $scCO_2$ conditions, the overall selectivity and permeability can be very different from those of the membrane (or skin layer) itself. Therefore, polarization effects need to be included in any analysis of mass transfer resistances during membrane transport.

Metz et al. [6] concluded that concentration polarization effects, enhanced by the relatively low H_2O diffusion across the feed gas boundary layer, compromise the water vapor permeability and H_2O/CO_2 selectivity already at low feed pressures. At constant temperature and increasing pressure, molecules start gathering more densely, leading to a reduced mean free path of motion, an increased molecular collision resulting in a lower diffusion coefficient. The relationship between the declining diffusion coefficient and increasing fluid density was also pointed out by Magalhães et al. [7]. Considering the high fluid density under $scCO_2$ conditions, up to 200 times higher compared to the low pressure experiments of Metz [6], it is expected that concentration polarization effects become even more dominant. Scholz et al. [5] analyzed non-ideal effects during gas permeation, including concentration polarization, the pressure drop along the flow channels and the Joule-Thomson effect. Even though we focused exclusively on the effect of concentration polarization, allowed maximum pressure drops along the flow channels are implicitly accounted for. Because of applying a sweep gas (in contrast to Schulz et al. [5]), the Joule-Thompson effect has been ignored during our simulations.

During the dehydration process of $scCO_2$ and when moving from the feed bulk to the permeate bulk solution, the water vapor (and CO_2) passes four layers in series: the feed boundary layer, the active skin layer, the porous membrane support and the permeate boundary layer, as depicted in Section 2.1 Transport model. The three highly water vapor permeable and H_2O/CO_2 selective membrane materials: SPEEK, Nafion® 117 and PEBAX® 1074, were included in this study. The aim of this simulation study is to delineate the contribution of each of these layers to the overall mass transport resistance. Recommendations for membrane material selection as well as process conditions to optimize the membrane-based dehydration will be discussed.

2. Theory

The membrane design considered in this study contains multiple flat sheet membranes arranged in parallel and separated by feed and permeate channels (Fig. 2). Ideally, the membrane is highly permeable for H_2O but not for $scCO_2$. As a result, humid $scCO_2$ that enters the feed channel, gets dehydrated and exits the feed channel as a dry $scCO_2$ stream ready for being reused as drying agent. A sweep gas, being pre-dried air, is used to maintain a high driving force for water vapor transport. A with water saturated $scCO_2$ feed stream, having pressures and temperatures of 13.0 MPa and 45 °C, is considered in this study.

2.1. Transport model

The system analyzed in this study is schematically depicted in Fig. 3. The product drying, hydrated $scCO_2$ is the bulk feed solution from which the water is transported via the feed boundary layer, (selective) skin layer of the membrane, porous support of the membrane, permeate boundary layer into the bulk permeate solution.

Assuming well-stirred conditions in the bulk solutions, the overall mass transfer resistance R_{ov} as well as the overall mass transfer coefficient k_{ov} can be represented by four mass flow resistances in series:

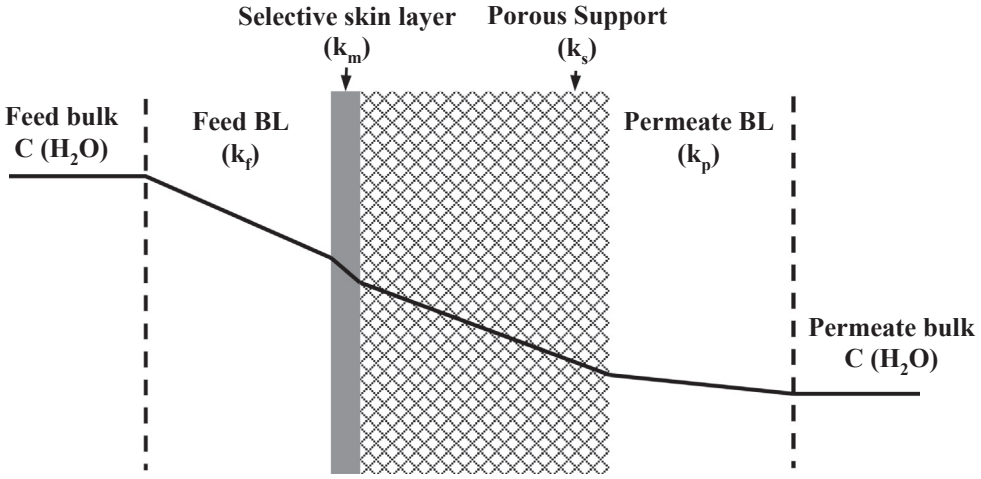

Fig. 3. H_2O concentration profile of a composite membrane and its fluid boundary layers. The resistance of each layer towards the transport of H_2O manifests itself in the specific concentration depletion within each layer.

$$R_{ov} = \frac{1}{k_{ov}} = \frac{1}{k_f} + \frac{1}{k_m} + \frac{1}{k_s} + \frac{1}{k_p} \tag{1}$$

including the mass transfer coefficient of the stagnant fluid boundary layer at the feed side k_f, the selective skin layer k_m, the porous support k_s and the stagnant fluid boundary layer at the permeate side k_p, all with the unit m/s.

2.1.1. Mass transfer coefficient of the skin layer

There are two expressions describing the flux of H_2O and CO_2 across the selective skin layer in Fig. 3, the first in terms of permeability P_i:

$$J_i = \frac{P_i}{l} \cdot \Delta f_i \tag{2}$$

where l represents the thickness of the skin layer (m) P_i the permeability coefficient, expressed in Barrer (1 Barrer = $7.5 \cdot 10^{-18}$ m^3(STP) m/(m^2 s Pa)) and Δf_i the driving force (Pa), being derived from the components fugacity of the supercritical and gaseous bulk phases of the feed and permeate side, respectively.

The second expression gives the flux in terms of mass transfer coefficient (k_i).

$$J_i = k_i \cdot \frac{V_{STP}}{R \cdot T} \cdot \Delta f_i \tag{3}$$

where J_i is the flux (m^3(STP)/m^2·s), k_i is the mass transfer coefficient (m/s), Δf_i the process driving force (Pa), T the process temperature (K), R the ideal gas constant (J/(mol·K)) and V_{STP} the molar volume at standard temperature and pressure (m^3(STP)/mol).

Combining Eqs. (1) and (2) correlates k_i and P_i:

$$k_i = \frac{P_i}{l} \cdot \frac{R \cdot T}{V_{STP}} \tag{4}$$

The k_m values for H_2O and CO_2 can be calculated using Eq. (4) and from the data in Table 1, showing the H_2O permeability and H_2O over CO_2 selectivity for three types of membranes: SPEEK, Nafion® 117 and PEBAX® 1074. We selected these three types due to their extremely high permeabilities towards water vapor [6] and their high H_2O over CO_2 selectivity compared to other currently existing membrane types. Further, Nafion® 117 and PEBAX® 1074 are commercially used for various drying applications [8,9]. SPEEK and PEBAX® 1074 on the other hand, have proven in months-long experiments to dehydrate flue gas under harsh corrosive conditions [10].

2.1.2. Mass transfer coefficient of the porous support layer

The flux through the porous support layer is a combination of diffusion-promoted flow and viscous flow [13]. At low pressures, as present at the permeate side, and high concentration gradients, the viscous flow is small compared to the diffusion-promoted flow, and is therefore neglected [13]. The mass transfer coefficient of the porous support is described by the reduced Dusty gas model [14]:

$$k_{s,i} = \frac{D_{comb,i} \cdot \varepsilon}{\tau \cdot l_{supp}} \tag{5}$$

where $D_{comb,i}$ is the combined diffusion coefficient (m^2/s), l_{supp} the porous support thickness (m), ε the support porosity (–) and τ the support tortuosity (–), approximated by Iversen et al. [15]

$$\tau = \frac{(2-\varepsilon)^2}{\varepsilon} \tag{6}$$

Table 2 lists the transport characteristics of the composite membrane used in this simulation study. The selected values for pore size, porosity and thickness of both dense and porous support layer of the membrane are all based on specifications of commercially available composite membranes [14].

With the support porosity, tortuosity and thickness known, Eq. (5) just requires the input of $D_{comb,i}$ (m^2/s). This parameter, in turn, is composed of two separate diffusion coefficients, D_{AB}, the binary diffusion coefficient (m^2/s) and $D_{knud,i}$, the Knudsen diffusion coefficient (m^2/s) [14]:

Table 1
H_2O permeability and H_2O/CO_2 selectivity of SPEEK, Nafion® 117 and PEBAX® 1074 membranes. The H_2O/CO_2 selectivity has been derived from the H_2O and CO_2 permeabilities. Data for SPEEK has been obtained from [10] (CO_2) and [6] (H_2O), data for Nafion® 117 from [11] (CO_2) and [12] (H_2O) and for PEBAX® 1074 from [10].

Polymer	Abbreviation	H_2O permeability (Barrer)	CO_2 permeability (Barrer)	H_2O/CO_2 selectivity (–)
Sulfonated polyetheretherketon	SPEEK	61,000	0.11	554,545
Perfluorosulfonic acid/Polytetrafluoroethylene copolymer	Nafion® 117	410,000	2.8	146,429
Poly(amide-12-b-ethylene oxide)	PEBAX® 1074	200,000	122	1639

Table 2
Process parameters for the composite membrane used for the simulations.

Process parameter	Value	Process parameter	Value
Process temperature	45 °C		
Pore size of the porous support	0.1 μm	Porosity of the support	0.7
Thickness porous support	120 μm	Thickness of the skin layer	1 μm

$$\frac{1}{D_{comb,i}} = \frac{1}{D_{knud,i}} + \frac{1}{D_{AB}} \tag{7}$$

The Knudsen diffusion coefficient is determined according to,

$$D_{knud,i} = \frac{2}{3}\cdot r_p \cdot \sqrt{\frac{8\cdot R\cdot T}{\pi \cdot M_i}} \tag{8}$$

where r_p is the pore radius of the porous support layer (m) and M_i is the molecular weight of the component i (kg/mol), T is the considered temperature (K) and R is the ideal gas constant (J/(mol K)).

As for the used sweep gas (dry air), we just consider the most abundant component in air, N_2 interacting with the permeating H_2O, thus present in the binary diffusion equation. Following Massman [16], the binary diffusion coefficient is expressed by the (empirical) relation:

$$D_{AB} = D_{AB,0}\cdot\left(\frac{p}{p_0}\right)\cdot\left(\frac{T_0}{T}\right)^{1.81} \tag{9}$$

where $D_{AB,0}$ is the binary diffusion coefficient (m^2/s) at 0.1013 MPa and 273.15 K ($2.178\cdot10^{-5}\,m^2/s$ for the H_2O/Air system), p the actual pressure (Pa), $p_0 = 0.1013$ MPa, T the actual temperature (K) and $T_0 = 273.15$ K.

2.1.3. Mass transfer coefficient of the boundary layers

Starting point for the mass transfer coefficient at the boundary layer at the feed side is the Sherwood number (*Sh*), under turbulent conditions defined by [17]:

$$Sh = 0.023\cdot Re^{0.8}\cdot Sc^{0.33} = \left(\frac{d_h\cdot k_{BL,i}}{D_{AB}}\right) \tag{10}$$

Here d_h is the hydraulic diameter of the boundary layer (m) and $k_{BL,i}$ is the mass transfer coefficients over the stagnant fluid boundary layer (m/s). The dimensionless Reynolds (Re) and Schmidt (Sc) numbers are defined as [18]:

$$Re = \frac{\rho\cdot v\cdot d_h}{\mu} \tag{11}$$

and

$$Sc = \frac{\mu}{\rho\cdot D_{AB}} \tag{12}$$

with ρ the fluid density (kg/m^3), v the fluid velocity (m/s), μ the dynamic viscosity (Pa s), d_h the hydraulic diameter (m) being twice the channel height and D_{AB} the continuum diffusion coefficient (m^2/s).

Eq. (8), taken of Massman [16], was used to determine D_{AB} for the low pressure permeate side, whereas a model developed by Magalhães et al. [7] was used to determine D_{AB} of the two component system H_2O/CO_2 at the feed side. Actually, our experimental conditions fall beyond the range in which Lito's model has been validated. However, given the fact that the model has been successfully applied to almost five hundred binary systems in the gas, liquid or $scCO_2$ state for a wide range of pressures and temperatures, we feel confident that application here is justified as well.

Calculation of Re and Sc requires knowledge of the density and dynamic viscosity, also under $scCO_2$ conditions. Table 3 shows values obtained from literature, for air and water (0.1 MPa and 45 °C) and $scCO_2$ (13.0 MPa and 45 °C), including the references. Worth to note, we found at least one website that allows the calculation of these parameters under a given set of experimental conditions. An example is given by [19] and [20]. The values obtained from this website were always in very close agreement with the values published in [21,22].

Table 3
Densities and viscosities of air [20] and water [19] at 45 °C and 0.1 MPa, and $scCO_2$ at 45 °C and 13.0 MPa [19]. Supercritical CO_2 shows higher Reynolds numbers than air and water at a given geometry and fluid velocity.

Fluid	Density ρ = [kg/m³]	Dynamic viscosity μ = [Pa s]
Air	1.10	$19.43\cdot10^{-6}$
$scCO_2$	693.7	$55.57\cdot10^{-6}$
H_2O	990.2	$59.61\cdot10^{-5}$

Table 4
Calculated Reynolds and Sherwood numbers and continuum diffusion coefficients for feed and permeate side, as used for the simulations.

Process parameter	Feed side value	Permeate side value
Fluid pressure	13.0 MPa	0.1 MPa
Flow channel height	0.8 mm	7 mm
Crossflow velocity	1.04 m/s	2.75 m/s
Reynolds number	20,828 (turbulent)	2160 (laminar)
Sherwood number	84.3	7.92
Continuum diffusion coefficient	$3.74\cdot10^{-8}\,m^2/s$	$2.91\cdot10^{-5}\,m^2/s$

Table 4 shows a number of process parameters used in and obtained from the simulation being: fluid pressure, flow channel height, cross flow velocity and others. The (maximum) pressure drop for the feed and sweep gas stream were set at 0.15 MPa and 5000 Pa, respectively to exclude any significant changes in both fluid properties due to their compression. These two pressure values were used as boundary conditions for the adjustment of the flow channel height at each side of the membrane. Listed fluid velocities in Table 4 resulted directly from the simulations. In addition, t contains the calculated Re and Sh numbers. The first is essential to justify the use of Eq. (10) as it demands the condition of turbulent flow to be fulfilled [17]. With a Re number of > 20,000, this is certainly the case.

As shown in Table 4, with a Re value of 2160, the flow regime at the permeate side of the membrane is laminar, implying Eq. (10) cannot be used. Instead two Sherwood numbers, differing in their boundary conditions, thus in their values, are used to describe the mass transport at laminar conditions, according to Skelland et al. [23]. In case of a uniform penetrant concentration along the permeate side Sh equals 7.60 whereas Sh is 8.23 in case of a uniform penetrant flux along the fluid-membrane interface. For the system considered here, we face an intermediate regime. Following Beusher et al. [13], the average of both Sh values (i.e., 7.92) was used.

Once Sh is known, $k_{BL,i}$ is calculaded according to:

$$k_{BL,i} = \frac{D_{AB}\cdot Sh}{d_h} \tag{13}$$

2.1.4. Calculation of driving force and fluxes

With all the individual mass transfer coefficients determined, Eq. (1) allows the calculation of the overall mass transfer coefficient for component i, $k_{ov,i}$. Apart from $k_{ov,i}$, calculation of fluxes requires calculation of the driving forces. The driving force Δf_i, for water vapor and CO_2 is given by the logarithmic mean difference of the components fugacity at the feed and permeate side:

$$\Delta f_i = \frac{(f_{0,i}^F - f_{0,i}^P) - (f_i{}^F - f_i{}^P)}{\ln\frac{f_{0,i}^F - f_{0,i}^P}{f_i{}^F - f_i{}^P}} \tag{14}$$

where $f_{0,i}^F$ and $f_i{}^F$ are the fugacities of the components in the feed and retentate stream and $f_{0,i}^P$ and $f_i{}^P$ are the fugacities of the components in

the sweep gas and permeate stream (Pa). At low pressures, apparent at the permeate side, gases behave fairly ideal and their partial pressure equals their corresponding fugacity.

Supercritical conditions are typified by high pressure and high temperature therefore the apparent fugacity was used instead of the partial pressure to describe the (non-ideal) fluid. The model developed by Spycher et al. [24] was used to determine the H_2O and CO_2 fugacity in the feed stream. The water activity of the supercritical feed stream entering the membrane module was assumed to be unity, implying a feed stream saturated with water. Assuming a dehydration of the feed solution of 85%, the water activity of the retentate was set at 0.15. The CO_2 fugacity in the feed was considered to be constant.

The Antoine equation [6] was used to convert the dew point temperature of the sweep gas (of +3 °C and 0.3 MPa) to its corresponding water vapor fugacity, assuming a sweep gas exit stream of 60% relative humidity. The CO_2 fugacity at the permeate side was considered to be negligible small compared to that of the feed side. By implication, the CO_2 driving force is essentially insensitive to the CO_2 fugacity of the permeate stream.

With both $k_{ov,i}$ and Δf_i, known, Eq. (15) gives the flux J_i (in m^3(STP)/m^2 s) of component i:

$$J_i = k_{ov,i} \cdot \frac{V_{STP}}{R \cdot T} \cdot \Delta f_i \tag{15}$$

2.2. Selectivity

The H_2O over CO_2 selectivity of the membrane (S_M) is defined as the ratio of the permeability coefficients:

$$S_{M,H_2O/CO_2} = \frac{P_{H_2O}}{P_{CO_2}} \tag{16}$$

The overall mass transfer coefficient (and resistance) for H_2O and CO_2 transport includes not only the membrane itself but also both boundary layers (Eq. (1). In analogy to Eq. (16), the ratio of the overall mass transfer coefficient for H_2O and CO_2 ($S_{OV,H_2O/CO_2}$) is given by:

$$S_{OV,H_2O/CO_2} = \frac{k_{ov,H_2O}}{k_{ov,CO_2}} \tag{17}$$

Due to e.g. concentration polarization effects, the selectivity predicted by $S_{OV,\ H2O/CO2}$ can significantly deviate from the selectivity represented by $S_{M,H_2O/CO_2}$. Finally, according to Eq. (3), the ratio of the flux of H_2O and CO_2 over the membrane ($S_{F,H_2O/CO_2}$) is given by:

$$S_{F,H_2O/CO_2} = \frac{k_{ov,H_2O} \cdot \Delta F_{H_2O}}{k_{ov,CO_2} \cdot \Delta F_{CO_2}} \tag{18}$$

3. Results and discussion

3.1. Delineating the overall mass transport resistance for water

Simulations were performed for three polymer membranes: SPEEK, Nafion® 117 and PEBAX® 1074, all with their distinctive properties as listed in Tables 1 and 2. SPEEK and Nafion® 117 are glassy polymers at room temperature and show exceptionally high H_2O/CO_2 selectivities compared to the elastomeric polymer PEBAX® 1074, whereas PEBAX® 1074 and Nafion® 117 show a water vapor permeability of 3 and 6 times higher than SPEEK, respectively.

Fig. 4 shows the calculated mass transfer resistance of the layers displayed in Fig. 3, with either the implementation of a SPEEK, Nafion® 117 or PEBAX® 1074 membrane.

Irrespective the membrane type used, the feed boundary layer forms by far the highest mass transfer resistance, comprising about 80% of the overall mass transfer resistance. Apparently, even the diminishing effect of high turbulence (Re = 20,800), as observed by Metz [6], cannot compensate the aforementioned feed boundary layer. To this end we concluded that the high fluid density substantially reduces the free path of motion of the water molecules and with that diffusive mass transport.

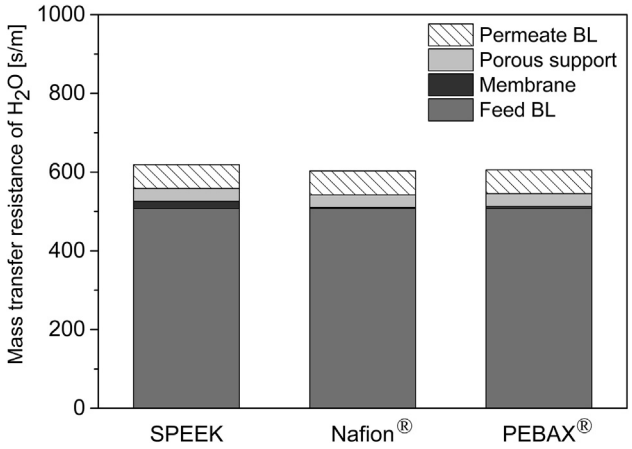

Fig. 4. H_2O mass transfer resistance of permeate boundary layer (BL), porous support, skin layer and feed boundary layer, calculated for three different composite membranes, SPEEK, *Nafion® 117* and PEBAX® 1074.

The second largest contributor to the overall mass transport resistance is the permeate boundary layer. Although the hydraulic diameter of the permeate canal, is about 9 times larger than those of the feed canal and its flow profile is laminar, it contributes for about 10% of the total mass transport resistance. Given the much lower fluid density at the permeate side, this outcome underlines the dominant effect of fluid density on the boundary layer resistance.

The porous support layer of thickness 120 µm contributes minor to the overall mass transfer resistance.

For all three membrane types, the layer showing the lowest mass transfer resistance is the dense, skin layer itself. This is a rather atypical outcome for a gas separation process as, in general, the thickness of the skin layer is the mass transfer limiting parameter. Our finding results directly from the combination of the exceptionally high water vapor permeability of these fairly thin skin layers and the $scCO_2$ condition, resulting in a high feed boundary layer resistance. Consequently, even though Nafion® 117 is six times more permeable for water vapor than SPEEK, it will only marginally improve the overall water permeance.

3.2. H_2O feed boundary resistance and fluid density as function of pressure and temperature

Given the high feed boundary resistance as outlined in the previous section, here we investigate strategies to lower this resistance by changing temperature and/or pressure. Fig. 5 displays the feed boundary resistance and fluid density in relation to feed pressure (left panel) and temperature (right panel). Values in Table 3 refer to process conditions of 13.0 MPa and 45 °C. To be consistent, the process temperature for the pressure profile was set at 45 °C whereas the process pressure for the temperature profile was set at 13.0 MPa. As for the effect of pressure (left panel of Fig. 5), fluid density and boundary layer resistance change in parallel as both parameters are affected by the reduction in free path of motion with increasing pressure. Both parameters increase till a pressure of around 11.0 MPa, after which the increase slightly flattens off. The temperature profile (right panel) also shows boundary resistance and fluid density change in parallel. This parallel change suggest that the effect of temperature is indirect and via the fluid density, which again leads, according to Magalhães et al. [7], to a reduction in free path of motion, and with that to a declined species diffusion within the fluid-membrane interface.

Both fluid density and feed boundary layer resistance decrease with temperature, with a flattening starting at a temperature around 70 °C. Pressure or temperature variation near the supercritical point results in

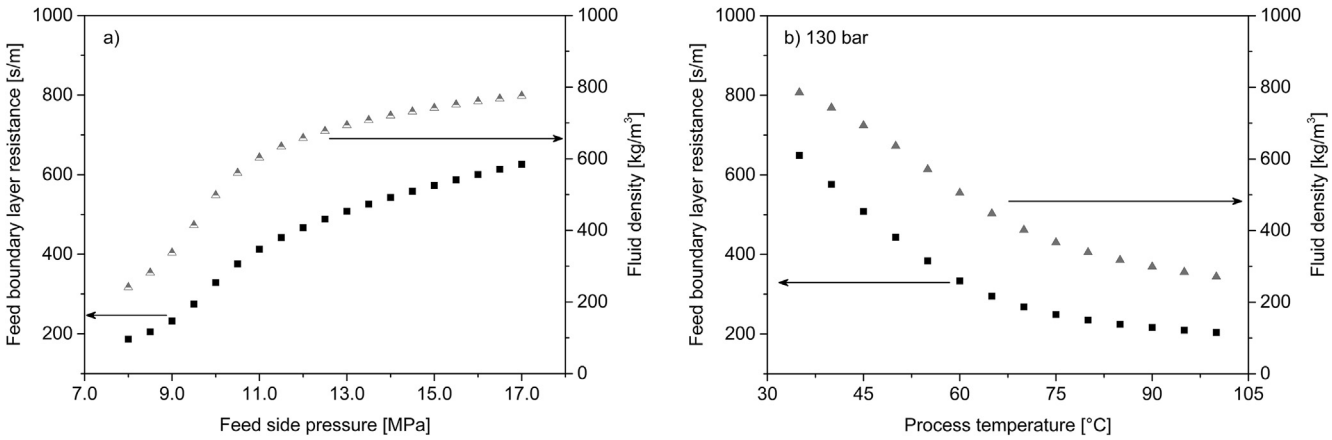

Fig. 5. Fluid density and feed boundary resistance as function of (a) feed pressure and (b) process temperature. Process parameters: the feed fluid velocity in (a) and (b) is 1.04 m/s, the temperature in (a) is 45 °C and the pressure in (b) is 13.0 MPa.

a more pronounced change in fluid density (and thus boundary layer resistance) due to its higher compressibility at this point [24]. This might be the root of the inflection points of the density and boundary layer resistance in the pressure profile.

As evident from Fig. 5, reducing the feed pressure from 13.0 MPa to 8.5 MPa while increasing the temperature from 45 °C to 100 °C would significantly diminish the boundary layer resistance with a factor 6 and thus improve the overall water vapor transport across the system. Despite the beneficial effects for the water vapor transport, the lower density leads to higher volume flow rates.

In analogy to Fig. 4 for H_2O, Fig. 6 shows the relative contribution of each transport layer to the overall mass transfer resistance for CO_2. Compared to Fig. 4, differences are striking. Firstly, not only are the overall mass transfer resistances for CO_2 much higher than those for H_2O, values for the three membranes vary widely.

The calculated mass transfer resistances for CO_2 are 9300, 403,500 and 10,269,800 s/m for PEBAX® 1074, Nafion® 117 and SPEEK, respectively. Note that for PEBAX® 1074, showing the lowest CO_2

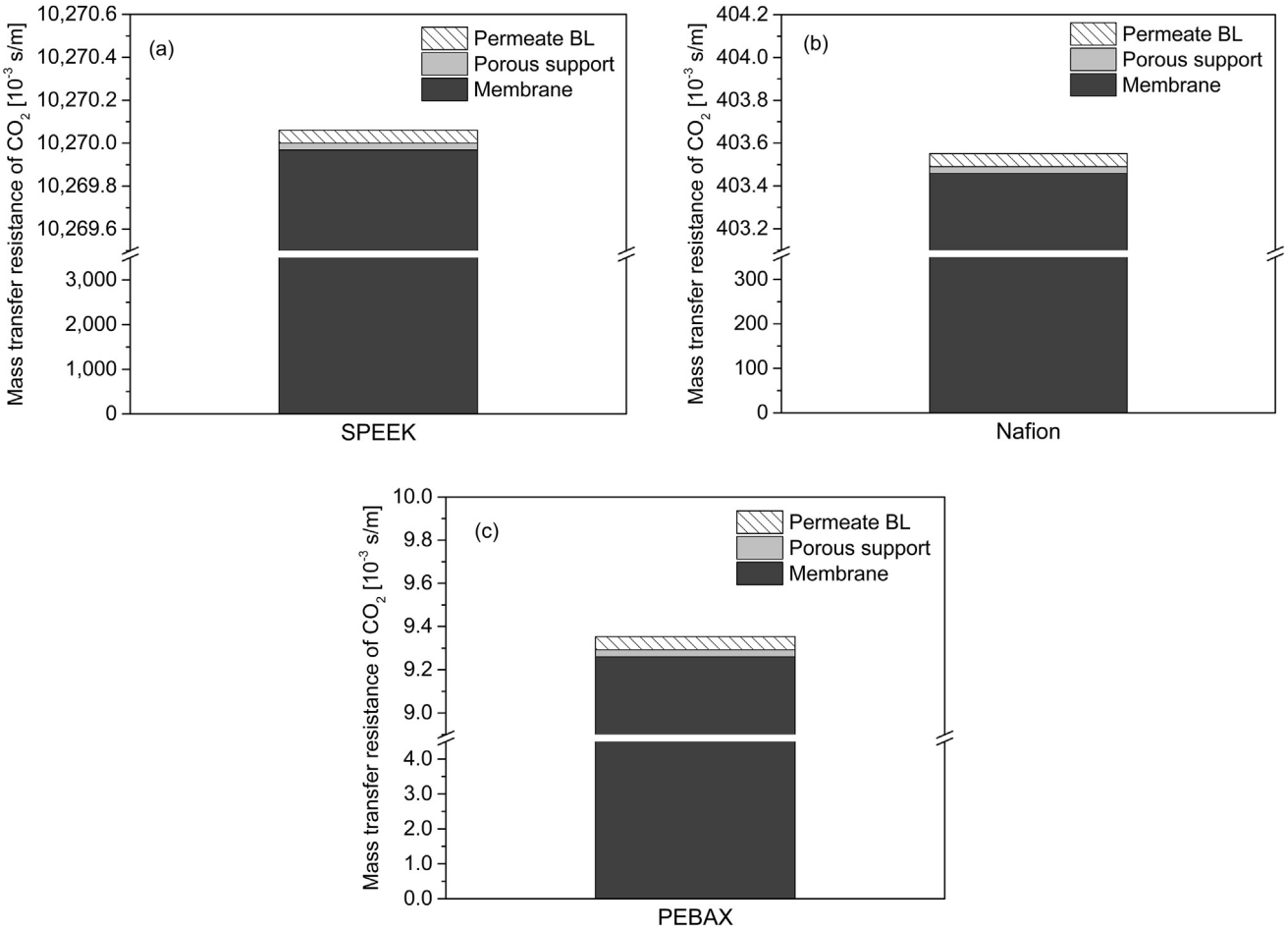

Fig. 6. CO_2 mass transfer resistance of permeate boundary layer (BL), porous support, skin layer and feed boundary layer, calculated for three different composite membranes, SPEEK (a), Nafion® 117 (b) and PEBAX® 1074 (c).

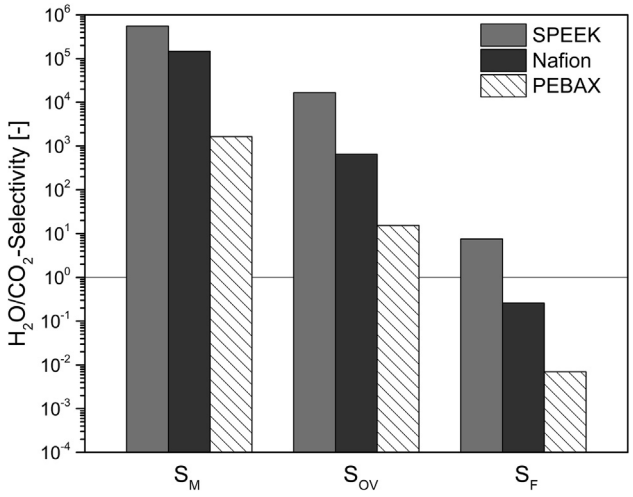

Fig. 7. Membrane selectivity, ratio of the overall mass transfer coefficient and flux ratio of H_2O over CO_2 for SPEEK, Nafion® 117 and PEBAX® 1074 at a feed pressure of 13.0 MPa and a temperature of 45 °C and a selective skin layer thickness of 1 μm.

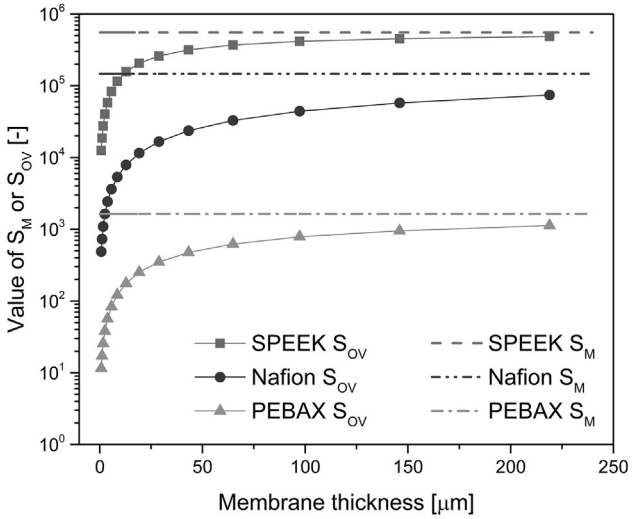

Fig. 8. The membrane H_2O/CO_2 selectivity (S_M) and the ratio of overall mass transfer resistances for H_2O and CO_2 (S_{OV}) plotted as function of skin layer thickness. A feed pressure of 13.0 MPa and a temperature of 45 °C is considered.

resistance, the value of 9300 s/m is already about 15 times the overall resistance for water vapor transport (Fig. 4). Secondly, due to the high $scCO_2$ concentration, the feed boundary layer resistance for CO_2 is non-existent (and for that reason not shown in Fig. 6). The consequence of this is that the CO_2 mass transfer resistance is dictated for more than 99% by the skin layer.

3.3. Selectivity

Fig. 7 shows the H_2O over CO_2 membrane selectivity (S_M), the ratio of the overall mass transfer resistance for H_2O and CO_2 (S_{OV}) and H_2O/CO_2 flux ratio (S_F), calculated for all three selected membrane materials. As shown by Eq. (16), the membrane selectivity reflects the ratio of the permeability for H_2O and CO_2. The relatively high H_2O over CO_2 membrane selectivity of SPEEK and Nafion® 117, in the range of 10^5–10^6, arises from the combined effect of a high water vapor permeability and a very low CO_2 permeability, see also Table 1. Even though the H_2O permeability of PEBAX® 1074 is comparable to that of SPEEK and Nafion® 117, the permeability for CO_2 of 122 Barrer is 2 to 3 orders of magnitude higher than for SPEEK and Nafion® 117, resulting in H_2O over CO_2 membrane selectivity of just 10^3.

As obvious from Fig. 7, the ratio of the overall mass transfer coefficient S_{OV} for H_2O and CO_2 is for all three membranes lower than the membrane selectivity S_M being solely based on the permeability ratio of the selective skin layer material itself. The reason is the dominance of the feed boundary layer resistance in the overall H_2O mass transfer resistance. In our simulations this effect is independent of the type of membrane. Therefore, differences in the overall mass transfer resistance between the three membrane types shown in Fig. 7 reflect more than anything else the differences in their CO_2 permeability as this parameter dominates the overall CO_2 mass transfer resistance.

Based on the S_M and S_{OV} values (all $\gg 1$) shown in Fig. 7, all three membrane types favor H_2O transport over CO_2 transport. This picture changes however dramatically when including driving forces in the analysis and investigating the actual flux ratio of H_2O and CO_2 (S_F) across the system. The large difference between S_{OV} and S_F values is caused by the large difference in driving force for H_2O and CO_2. According to Spycher [24], water vapor-saturated CO_2 at the feed side of 13.0 MPa and 45 °C has a CO_2 and H_2O fugacity of 6.76 MPa and 0.01 MPa, respectively. Given the virtually zero H_2O and CO_2 fugacity at the permeate side, this large difference in fugacity translates in a driving force for CO_2 that is almost 700 times (=67.6/0.1) higher than the driving force for H_2O. As a result, S_F becomes < 1 for Nafion® 117 and PEBAX® 1074 membranes, implying that the membrane actually passes more CO_2 than H_2O. Only the SPEEK membranes permeates given more H_2O than CO_2. In conclusion, this outcome shows that a very H_2O/CO_2 selective skin layer, as is the case for Nafion® 117 and PEBAX® 1074, does not necessary lead to (desired) low CO_2 crossover and high H_2O fluxes over the membrane ($S_F \gg 1$). Strong concentration polarizations effects and an unfavorable driving force ratio can severely reduce or even inverse the H_2O/CO_2 flux ratio. Given the membrane polymers included in this study as well as the process conditions, SPEEK would be the material of choice since even under the given $scCO_2$ conditions the SPEEK membrane shows a S_F value of almost 10, indicating the H_2O flux is almost 10-times higher than the CO_2 flux. This means that during the dehydration process with SPEEK membranes the CO_2 loss is limited.

3.3.1. Effect of skin layer thickness

The mass transfer over the feed boundary layer is dictating for the H_2O transport, while the selective skin layer controls the CO_2 mass transfer. Fig. 8 shows the effect of skin layer thickness on the overall mass transfer coefficient.

Increasing the skin layer thickness from 1 μm up to 250 μm, increases S_{OV}. Up to 25 μm this increase is about 1.5 orders of magnitude. Above 25 μm it levels asymptotically approaching S_M. The initial increase reflects the sensitivity of the overall mass transfer resistance for CO_2 towards skin layer thickness with the one for H_2O remaining essentially unaffected as for H_2O the feed boundary layer remains by far the dominant resistance.

However, upon a further increase of the skin layer thickness, the skin layer resistance towards H_2O transport becomes more pronounced, even to the point that it supersedes the feed boundary layer as the mass transfer limiting layer. As a result, for both H_2O and CO_2 the membrane resistance becomes the dominating term in the overall mass transfer resistance with the value of S_{OV} asymptotically approaching that of S_M.

Even though the behavior outlined above is valid for all three membrane types, they differ in detail. For SPEEK S_M and S_{OV} are already fairly the same at a skin layer thickness of 150 μm. In contrast, at the same skin layer thickness Nafion® 117 still demonstrates a significant discrepancy between these two parameters, whereas PEBAX® 1074 behaves intermediately. This diverse behavior is rooted in differences in water permeability, 61,000 Barrer for SPEEK and 410,000 Barrer for Nafion® 117. As a consequence, when increasing the skin

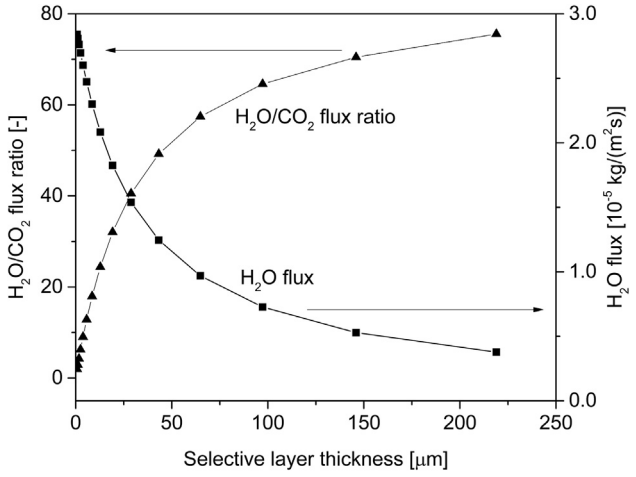

Fig. 9. The H_2O/CO_2 flux ratio and H_2O flux as function of the thickness of a selective SPEEK skin layer at pressure of 13.0 MPa and a temperature of 45 °C of the saturated feed stream. The thickness of the porous support is kept constant.

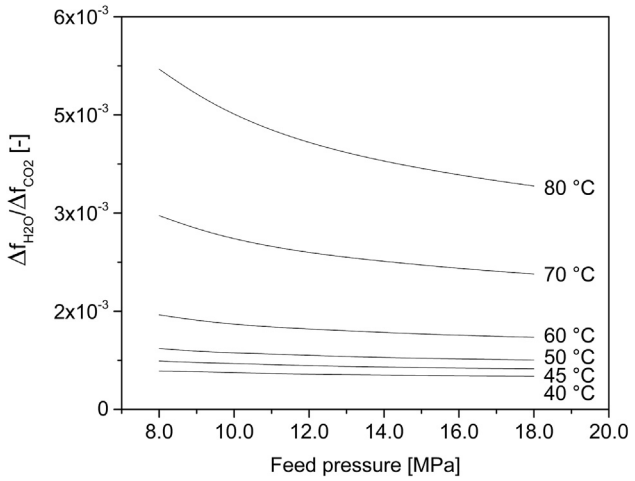

Fig. 10. The H_2O/CO_2 driving force ratio as function of fluid temperature and pressure. The water activity in the feed stream is 1 and 0.15 in the retentate stream. A dew point of 3 °C at 0.3 MPa is considered for the sweep gas while a water activity of 0.6 is considered for the permeate stream.

layer thickness, a SPEEK-based membrane becomes limiting towards the transport of H_2O already at a much lower skin layer thickness than its Nafion® 117 counterpart.

To exemplify this in more detail, Fig. 9 displays the H_2O/CO_2 flux ratio and the H_2O flux, both plotted for a SPEEK membrane of various thickness, and at a feed pressure of 13.0 MPa and temperature of 45 °C. A low skin layer thickness leads to severe CO_2 losses. This effect is also pronounced by the low H_2O/CO_2 flux ratio. To compensate for this CO_2 loss, CO_2 refill, is demanded therefore installing thicker membranes is preferred from the CO_2 perspective. On the other hand, it might also not be cost-effective to install membranes with very thick skin layers. The substantially lower H_2O flux would demand a larger membrane area thereby inflating investment costs. Optimization of skin layer thickness resulting in total cost minimization is the focus of current investigation.

3.3.2. Driving force

As evident from Eq. (15), the H_2O and CO_2 flux depends on the respective driving force. Consequently, the flux ratio can not only be manipulated by parameters affecting (the ratio of) mass transfer resistances but also by those affecting (the ratio of) driving forces. In this section, we will explore the later in more detail in order to gain insight how to combine a high H_2O flux with a low CO_2 crossover. Changing the fluid properties by changing pressure and/or temperature affects the fugacities of CO_2 and H_2O and in addition latter's solubility in CO_2. Fig. 10 displays the ratio of isothermal driving force for H_2O and CO_2 in the H_2O-saturated CO_2 feed stream, each calculated using Eq. (14), as a function of fluid pressure, and at various temperatures.

As shown in Fig. 10, the driving force ratio strongly depends on fluid temperature, an effect related to the H_2O solubility/fugacity enhancing effect of the temperature. In addition, pressure increase lowers the H_2O and CO_2 driving force ratio, an effect more pronounced at elevated temperatures and possibly caused by a disproportional increase of the CO_2 fugacity with increasing pressure compared to the increase of H_2O fugacity [24]. Increasing the process temperature from 45 °C to 70 °C, combined with a pressure reduction from 13.0 MPa to 10.0 MPa, enhances the H_2O/CO_2-driving force ratio almost a factor 3 (see Fig. 10), resulting in a similar increase of the H_2O/CO_2 flux ratio. In effect, such a change in process conditions would result in a 75% reduction of CO_2 loss while maintaining the H_2O flux.

3.4. Summary of all discussed effects

The H_2O/CO_2 flux ratio can not only be manipulated by choice of membrane material and skin layer thickness but also by the process pressure and temperature. Fig. 11 compiles the possible effects of these parameters on the (intrinsic) membrane selectivity (S_M), ratio of the overall mass transfer coefficient (S_{OV}) and flux ratio (S_F). Given SPEEK as material of choice, three different dehydration systems are considered:

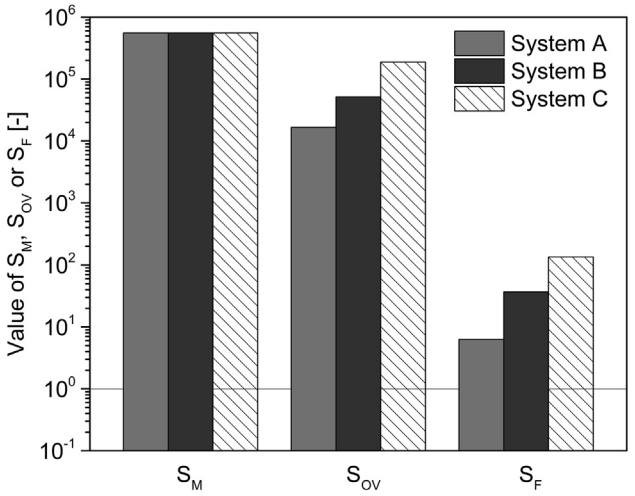

Fig. 11. Membrane selectivity, ratio of the overall mass transfer coefficient and H_2O/CO_2 flux ratio displayed for three different dehydration systems, all three based on SPEEK. Skin layer thickness: 1 μm for system A and 5 μm for systems B and C. Feed pressure and temperature: 13.0 MPa and 45 °C for systems A and B and 10.0 MPa and 70 °C for system C.

System A with a skin layer thickness of 1 μm and a feed pressure and temperature of 13.0 MPa and 45 °C, respectively. This system represents the default state which is used as a benchmark for the other systems.

System B with an increased skin layer thickness of 5 μm but the same feed pressure and temperature as in A, 13.0 MPa and 45 °C, respectively.

System C with the same skin layer thickness as in B, 5 μm, but with a decreased feed pressure and an increased temperature of 10.0 MPa and 70 °C, respectively.

Since all three systems are SPEEK-based, the (intrinsic) membrane selectivity is the same. Regarding the ratio of overall mass transfer resistance (S_{OV}), Fig. 11 shows an incremental increase when moving from system A to system B. The jump seen from system A to system B reflects the increase of skin layer thickness from 1 to 5 μm and the

resulting disproportional increase of CO_2's the mass transfer resistance compared to those of H_2O, as discussed previously (Fig. 8). The difference between the S_{OV} values of system B and C is the result of the increased temperature, from 45 to 70 °C, and lower pressure, from 13.0 to 10.0 MPa (see Fig. 11). Both adjustments of the process conditions lower the density of the supercritical fluid and by that improving the diffusion of water across the feed boundary layer.

Finally, most relevant is of course how these considered parameters translate in the overall performance of the system, i.e., the H_2O/CO_2 flux ratio, indicated by the S_F value. As shown in Fig. 7, the large difference in driving force for H_2O and CO_2 cancels out for most part the huge differences in S_M and, to a slightly lesser extent, S_{OV} values, resulting in S_F values ranging from approximately $5 \cdot 10^{-3}$ (for PEBAX® 1074) to 8 (for SPEEK). As the driving forces in Fig. 11 for systems A and B are the same, the observed increase in S_{OV} and S_F can solely be attributed to the effect of increased skin layer thickness, affecting predominantly the CO_2 permeance. As discussed in Fig. 10, lowering the feed pressure and increasing the feed temperature increases the H_2O/CO_2 driving force ratio, and thus H_2O/CO_2 flux ratio as well. This effect, in turn, is responsible for the difference shown between systems B and C. Comparing systems A and C, it can be concluded that increasing the skin layer thickness from 1 to 5 μm, while lowering the pressure from 13.0 to 10.0 MPa and increasing the temperature from 45 to 70 °C, increases the H_2O/CO_2 flux ratio up to almost 20 times.

4. Conclusions

The specific flow pattern across membranes depends on the geometry of the system. For that reason, here we consider the (relatively simple) mass transfer behavior of flat sheet membranes, depicted in Fig. 2. Despite their different geometry and more complex flow pattern, we nevertheless expect that conclusion can be (partly) extrapolated to outside-in hollow fiber membranes.

The system's performance of a $scCO_2$ dehydration unit was assessed by implementing a polymeric membrane based on either SPEEK, Nafion® 117 or PEBAX® 1074, all three materials are combining a very high H_2O permeability with a high H_2O over CO_2 membrane selectivity. Apart from membrane material, the system's performance, with the H_2O/CO_2 flux ratio as decisive criterion, was tested for skin layer thickness and the effects of feed pressure and temperature. One of the main findings of the analysis is that the feed boundary layer resistance is by far the principal term in the overall mass transfer resistance for H_2O. In contrast, the intrinsic membrane permeability towards CO_2 dominates the overall mass transfer resistance for CO_2. Together with the huge difference in driving force for CO_2 and H_2O this leads to H_2O/CO_2 flux ratios orders of magnitude lower than suggested by the S_M values, based solely on the membrane permeability for H_2O and CO_2. In case of Nafion® 117 and PEBAX® 1074 the H_2O/CO_2 flux ratio even lies below unity making CO_2 instead of H_2O the dominant species in the permeate. Which means high CO_2 loss during the regeneration process, thus making the process CO_2 selective.

Because of the above and given the $scCO_2$ process conditions and driving forces, membrane selection is based on a low CO_2 permeance rather than on high H_2O permeance. This consideration defines SPEEK as the preferred material for this specific application. In addition to the chosen membrane material, the thickness of the skin layer has a profound effect on CO_2 permeance as well, balancing between high permeance/high CO_2 losses for a thin layer and low permeance/large required membrane areas for a relatively thick layer. Common sense predicts an optimum thickness in terms of operational and investment costs. In addition to membrane properties, process conditions will greatly affect the S_F values. For a SPEEK membrane, increasing the skin layer thickness from 1 to 5 μm, lowering the feed pressure from 13.0 to 10.0 MPa and increasing the temperature from 45 to 70 °C, increases S_F almost 20-fold. System optimization, including effects of skin layer thickness as well as feed pressure and temperature, is the focus of future research.

Acknowledgements

This work was performed in the cooperation framework of Wetsus, European Centre of Excellence for Sustainable Water Technology (www.wetsus.nl). Wetsus is co-funded by the Dutch Ministry of Economic Affairs and Ministry of Infrastructure and Environment, the European Union Regional Development Fund, the Province of Fryslân, and the Northern Netherlands Provinces. The authors like to thank the participants of the research theme Dehydration (Feyecon, Avebe) for the fruitful discussions and their financial support.

References

[1] S. Khalloufi, C. Almeida-Rivera, P. Bongers, Supercritical-CO_2 drying of foodstuffs in packed beds: Experimental validation of a mathematical model and sensitive analysis, J. Food Eng. 96 (1) (2010) 141–150.
[2] A. Clifford, Fundamentals of Supercritical Fluids, Oxford University Press, New York, USA, 1998.
[3] Z.K. Brown, P.J. Fryer, I.T. Norton, S. Bakalis, R.H. Bridson, Drying of foods using supercritical carbon dioxide — Investigations with carrot, Innov. Food Sci. Emerg. Technol. 9 (3) (Jul. 2008) 280–289.
[4] T. Lohaus, M. Scholz, B.T. Koziara, N.E. Benes, M. Wessling, Drying of supercritical carbon dioxide with membrane processes, J. Supercrit. Fluids 98 (2015) 137–146.
[5] M. Scholz, T. Harlacher, T. Melin, M. Wessling, Modeling gas permeation by linking nonideal effects, Ind. Eng. Chem. Res. 52 (3) (2013) 1079–1088.
[6] S.J. Metz, W.J.C. Van De Ven, J. Potreck, M.H.V. Mulder, M. Wessling, Transport of water vapor and inert gas mixtures through highly selective and highly permeable polymer membranes, J. Memb. Sci. 251 (1–2) (2005) 29–41.
[7] A.L. Magalhães, P.F. Lito, F.A. Da Silva, C.M. Silva, Simple and accurate correlations for diffusion coefficients of solutes in liquids and supercritical fluids over wide ranges of temperature and density, J. Supercrit. Fluids 76 (2013) 94–114.
[8] Chromservis, "Nafion dryers." [Online]. Available: https://www.chromservis.eu/i/nafion-dryers?lang=EN. [Accessed: 12-Jun-2018].
[9] A. Group, "Breathable Films." [Online]. Available: https://www.extrememateials-arkema.com/en/markets-and-applications/chemical-industry-and-general-industry/breathable-films/. [Accessed: 12-Jun-2018].
[10] H. Sijbesma, K. Nymeijer, R. van Marwijk, R. Heijboer, J. Potreck, M. Wessling, Flue gas dehydration using polymer membranes, J. Memb. Sci. 313 (1–2) (Apr. 2008) 263–276.
[11] S.H. Choi, M.S. Qahtani, E.A. Qasem, Multilayer thin-film composite membranes for helium enrichment, J. Membr. Sci. 553 (2018) 180–188.
[12] H. Lin, et al., Dehydration of natural gas using membranes. Part I: Composite membranes, J. Memb. Sci. 413–414 (2012) 70–81.
[13] U. Beuscher, C.H. Gooding, The influence of the porous support layer of composite membranes on the separation of binary gas mixtures, J. Memb. Sci. 152 (1) (1999) 99–116.
[14] M. Dingemans, et al., Mass transfer characteristics for VOC permeation through flat sheet porous and composite membranes: The impact of the different membrane layers on the overall membrane resistance, J. Memb. Sci. 322 (1) (2008) 234–242.
[15] S.B. Iversen, V.K. Bhatia, K. Dam-Johansen, G. Jonsson, Characterization of microporous membranes for use in membrane contactors, J. Memb. Sci. 130 (1–2) (1997) 205–217.
[16] W.J. Massman, A review of the molecular diffusivities of H_2O, CO_2, CH_4, CO, O_3, SO_2, NH_3, N_2O, NO, and NO_2 in air, O_2 and N_2 near STP, Atmos. Environ. 32 (6) (1998) 1111–1127.
[17] G.B. Van Den Berg, I.G. Racz, C.A. Smolders, Mass transfer coefficients in cross-flow ultrafiltration, J. Memb. Sci. 47 (1–2) (1989) 25–51.
[18] R.B. Bird, W.E. Stewart, E. Lightfoot, Transport Phenomena, John Wiley & Sons Ltd, New York, USA, 1960.
[19] Thermophysical Properties of Fluid Systems - NIST: National Institute of Standards and Technology, 2016. [Online]. Available: http://webbook.nist.gov/chemistry/fluid/. [Accessed: 05-Apr-2017].
[20] B. Wischnewski, Calculation of thermodynamic state varibales of air. [Online]. Available: http://www.peacesoftware.de/einigewerte/luft_e.htm. [Accessed: 09-Jun-2017].
[21] R. Span, W. Wagner, A new equation of state for carbon dioxide covering the fluid region from the triple-point temperature to 1100 K at pressures up to 800 MPa, J. Phys. Chem. Ref. Data, Bochum, Germany (1996) 1509–1596.
[22] P.T. Tsilingiris, Thermophysical and transport properties of humid air at temperature range between 0 and 100 °C, Energy Convers. Manage. 49 (5) (2008) 1098–1110.
[23] K.K. Sirkar, Separation of Molecules, Macromolecules and Particles: Principles, Phenomena and Processes, Cambridge University Press, Cambridge, UK, 2014.
[24] N. Spycher, K. Pruess, J. Ennis-King, CO_2-H_2O mixtures in the geological sequestration of CO_2. I. Assessment and calculation of mutual solubilities from 12 to 100 °C and up to 600 bar, Geochim. Cosmochim. Acta 67 (16) (2003) 3015–3031.